nature geoscience

ARTICLES

PUBLISHED ONLINE: 20 FEBRUARY 2017 | DOI: 10.1038/NGEO2896

Non-chondritic iron isotope ratios in planetary mantles as a result of core formation

Stephen M. Elardo* and Anat Shahar

Information about the materials and conditions involved in planetary formation and differentiation in the early Solar System is recorded in iron isotope ratios. Samples from Earth, the Moon, Mars and the asteroid Vesta reveal significant variations in iron isotope ratios, but the sources of these variations remain uncertain. Here we present experiments that demonstrate that under the conditions of planetary core formation expected for the Moon, Mars and Vesta, iron isotopes fractionate between metal and silicate due to the presence of nickel, and enrich the bodies' mantles in isotopically light iron. However, the effect of nickel diminishes at higher temperatures: under conditions expected for Earth's core formation, we infer little fractionation of iron isotopes. From our experimental results and existing conceptual models of magma ocean crystallization and mantle partial melting, we find that nickel-induced fractionation can explain iron isotope variability found in planetary samples without invoking nebular or accretionary processes. We suggest that near-chondritic iron isotope ratios of basalts from Mars and Vesta, as well as the most primitive lunar basalts, were achieved by melting of isotopically light mantles, whereas the heavy iron isotope ratios of terrestrial ocean floor basalts are the result of melting of near-chondritic Earth mantle.

Understanding the origins of isotope fractionations in planetary materials is essential because they have the potential to record information about the conditions of accretion and differentiation of the terrestrial planets. For example, isotope ratios provide some of the strongest evidence available for the origin of the Earth–Moon system in a giant impact[1–3]. Previous studies have revealed that iron (Fe) stable isotope ratios in planetary materials, expressed as δ^{57}Fe (normalized ^{57}Fe/^{54}Fe relative to the international standard IRMM-014 in per mil units), show significant variation[4–14] (Fig. 1). Carbonaceous, ordinary and enstatite chondrites, primitive meteorites thought to constitute the main building blocks of the planets and asteroids, have an average δ^{57}Fe of 0.006 ± 0.022‰ (ref. 11) (2σ of weighted mean). Samples of Earth's oceanic peridotite upper mantle have a very similar composition (0.040 ± 0.040‰) (ref. 8) to chondrites. Basalts found along mid-ocean ridges (MORBs), which are partial melts of Earth's upper mantle, have heavier δ^{57}Fe (0.151 ± 0.010‰) compared with the peridotites from which they melted[7,8,11]. Shergottites and eucrites, however, meteoritic samples of basalts from Mars and the asteroid 4 Vesta respectively, have iron isotope compositions lighter than MORBs that are more similar to the chondrites[4–6,9,14], averaging 0.013 ± 0.008‰ and 0.034 ± 0.016‰, respectively. Lunar basalts span a wide range in δ^{57}Fe from chondritic values of -0.03‰ ± 0.05‰ in the primitive Apollo 15 green glasses[4] to heavier compositions observed in the more geochemically evolved low-titanium (Ti) and high-Ti basalts, averaging 0.107 ± 0.031‰ and 0.266 ± 0.029‰ (refs 4,5,10), respectively. Interestingly, despite planetary silicate samples having chondritic or heavy Fe isotope ratios, magmatic iron meteorites, which are thought to represent the cores of extinct planetesimals[15], also have a heavy average δ^{57}Fe of 0.127 ± 0.026‰ (refs 12,13).

The causes of these large differences among planetary materials are not yet fully understood. The similarity in δ^{57}Fe between shergottites, eucrites and chondrites has led to the suggestion that the δ^{57}Fe of bulk Earth and Moon were made heavier by vaporization and condensation during the giant impact[4,16], greater degrees of volatile element depletion during accretion[14], and/or the disproportionation of Fe^{2+} by bridgmanite in the deep Earth[17]. Other studies have invoked isotopic fractionation during core formation[6,18,19]. Early experimental studies suggested that Fe isotope fractionation between silicate and Fe metal would not be resolvable with current analytical capabilities[20,21]. However, Shahar *et al.*[22] found that as S enters Fe–Ni cores at pressure and temperature conditions relevant to small planets/asteroids or a shallow terrestrial magma ocean, it induces a clearly resolvable fractionation of Fe isotopes that scales with the S content of the core. Despite this finding, the presence of S in the cores of Earth and other planetary bodies in significant quantities is highly contested[23] and experiments that isolate the effects of Ni and other light elements do not exist.

Iron isotope experiments to simulate core formation

We conducted metal–silicate equilibration experiments in graphite containers to constrain equilibrium Fe isotope fractionation during core formation. By using graphite and varying the Ni content of our experiments, we were able to assess the effects of both C and Ni on Fe isotope fractionation. These experiments were conducted at 1,850 °C and 1 GPa to approximate the conditions of core formation relevant for smaller bodies such as the Moon, Mars and Vesta. The silicate was a peridotite-like composition and was combined with pure Fe metal or mixtures of Fe and Ni metals. The peridotite was spiked with ^{54}Fe such that isotopic equilibrium could be assessed with the three-isotope exchange method[24] (see Methods and Supplementary Figs 1 and 2).

The results of our experiments show that at C saturation the $\Delta^{57}Fe_{Core-Mantle}$ (that is, $\delta^{57}Fe_{Metal} - \delta^{57}Fe_{Silicate}$) is slightly negative but three of the four experiments are within analytical error of 0‰ (Fig. 2 and Supplementary Tables 1 and 2). This shows that the presence of C in planetary cores would not result in significant Fe isotope fractionation. However, our Ni-bearing

Geophysical Laboratory, Carnegie Institution of Washington, Washington DC 20015, USA. *e-mail: selardo@carnegiescience.edu

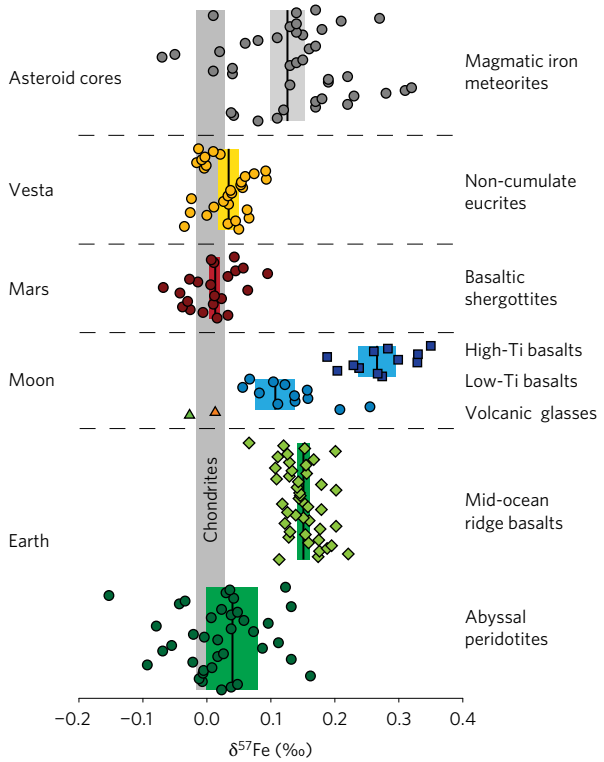

Figure 1 | The Fe isotopic compositions of planetary materials. The grey and coloured bars show the error-weighted means and 95% confidence intervals for chondritic meteorites and planetary sample groupings (values discussed in text). Data sources are referenced in the text. The typical uncertainty on MC-ICP-MS measurements of δ^{57}Fe is ~0.05‰ (ref. 11).

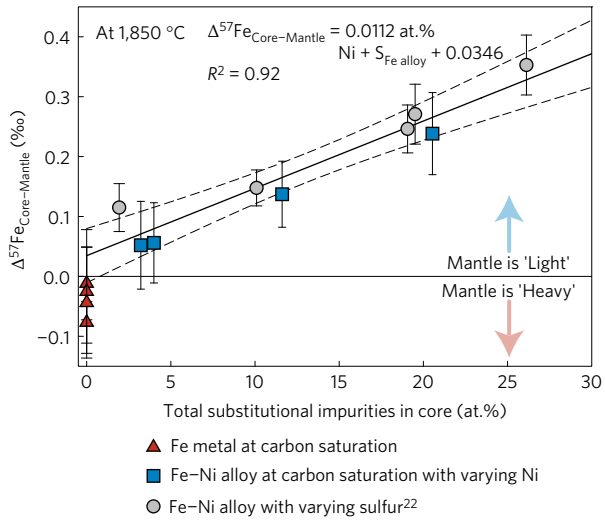

Figure 2 | Results of metal–silicate equilibration experiments. The $\Delta^{57}Fe_{Core-Mantle}$ of each experiment is shown as a function of the at.% of elements (that is, Ni and S) that substitute for Fe atoms in the Fe alloy structure. Elements such as C that reside in interstitial sites in the alloy plot at 0 at.%. Triangles and squares are data from the present study. Circles are data from Shahar *et al.*[22] and were recalculated at 1,850 °C. Error bars are 2 × s.e.m. (Supplementary Information). The solid line represents a linear regression (equation shown) of the Ni- and S-bearing experiments and the dashed curves represent the 95% confidence interval.

experiments show a clearly resolvable trend in $\Delta^{57}Fe_{Core-Mantle}$ that correlates with the Ni concentration of the Fe alloy (Fig. 2). This trend is indistinguishable within error from the S-controlled trend from Shahar *et al.*[22] and suggests a mechanism for these fractionations. At the conditions investigated, Ni and S substitute for Fe atoms in the alloy structure, whereas C partitions into interstitial sites[25]. This suggests that the substitution of Ni and S for Fe has a greater effect on the average bonding environment of Fe atoms in the alloy. In general, stiffer bonds concentrate heavier isotopes, and since liquids retain short-range order, the molten alloys relevant to core formation should retain the nearest-neighbour structural properties of solid alloys. The direction of this fractionation trend indicates that cores become isotopically heavier and bulk mantles will become lighter relative to the bulk planetary isotopic composition.

The iron isotopic composition of planetary mantles

The importance of these results is twofold. Firstly, a Ni-controlled fractionation will be ubiquitous in the Solar System and does not require the presence of any particular light element in a planetary core, although S enhances the overall fractionation. Chondritic Ni abundances and the metal–silicate partitioning of Ni[26] make it a cosmochemical certainty that any planet or asteroid that has undergone core formation will contain Ni in its core and will thus be subject to this fractionation. Secondly, this fractionation can potentially explain the differences in the δ^{57}Fe of planetary basalts when its effect on bulk mantle composition is considered. We have calculated the range in possible bulk mantle δ^{57}Fe for Earth, the Moon, Mars and Vesta using the isotope mass balance relationship,

$$\delta^{57}Fe_{Bulk\ Planet} = \delta^{57}Fe_{Mantle} \times f Fe_{Mantle} + \delta^{57}Fe_{Core} \times f Fe_{Core} \quad (1)$$

where fFe is the mass fraction of Fe in either the mantle or core after differentiation. Equation (1) can be rearranged to calculate the $\delta^{57}Fe_{Mantle}$ using our experimentally determined $\Delta^{57}Fe_{Core-Mantle}$.

$$\delta^{57}Fe_{Bulk\ Planet} = (\Delta^{57}Fe_{Core-Mantle} + \delta^{57}Fe_{Mantle}) \times (1 - f Fe_{Mantle}) + \delta^{57}Fe_{Mantle} \times f Fe_{Mantle} \quad (2)$$

We assume that $\delta^{57}Fe_{Bulk\ Planet}$ is equivalent to the chondritic value of ~0‰. The magnitude of $\Delta^{57}Fe_{Core-Mantle}$ at 1,850 °C is determined from a linear regression of the Ni- and S-bearing experiments (Fig. 2). The Ni content of Earth's core is assumed to be 4.4 at.% (ref. 27) and we consider the endmember cases where Earth's core is S-free and where S is solely responsible for a 10 wt% core density deficit. We have considered the full range in estimated core Ni and S contents from geochemical models for the Moon, Mars and Vesta[28–32]. Core formation temperature estimates for Earth depend on how accretion is modelled. Continuous accretion models are consistent with average temperatures of ~2,700 °C and single step models favour temperatures of ~2,900 °C to 3,600 °C (refs 33,34), though much hotter temperatures are possible[35]. Core formation temperature ranges for the Moon, Mars and Vesta are derived from geochemical models[28,36–39]. Since all equilibrium mass-dependent isotopic fractionation is proportional to $1/T^2$, we have used this relationship to extrapolate over the full range of core–mantle equilibration temperatures. The $f Fe_{Mantle}$ is calculated using estimates of core and mantle mass fractions[29,36,40] and is adjusted for the range in Ni and S contents used to calculate $\Delta^{57}Fe_{Core-Mantle}$ (see Supplementary Table 3 for a full listing of model parameters).

Our results predict that the bulk silicate mantles of the Moon, Mars and Vesta should have δ^{57}Fe compositions significantly below the chondritic average. The $\delta^{57}Fe_{Mantle}$ estimates range from −0.01‰ to −0.12‰ for the Moon, from −0.06‰ to −0.33‰ for Mars, and from −0.09‰ to −0.35‰ for Vesta (Fig. 3). We include calculations for Earth's mantle for completeness; however, we do not expect the results to be geologically meaningful. It has been shown that in Earth's deep interior the increased pressure results

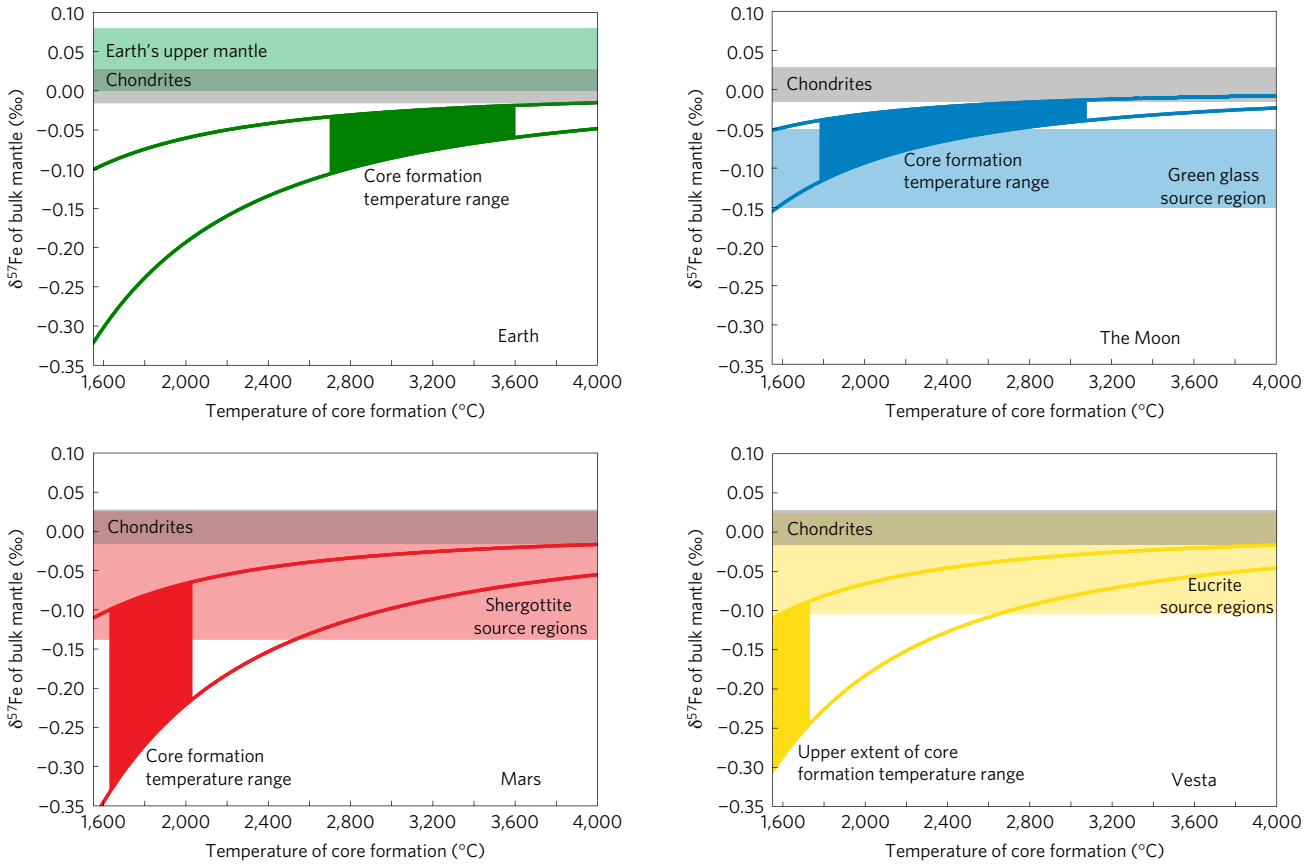

Figure 3 | The range in Fe isotopic compositions of bulk planetary mantles predicted from core formation models. The solid curves are the upper and lower limits on the δ^{57}Fe of planetary mantles calculated using equation (2) and parameters in Supplementary Table 3 as a function of core–mantle equilibration temperature. Solid shaded regions between the curves are the mantle values predicted over the estimated core formation temperature range specific to each planet. Coloured fields are the range for terrestrial abyssal peridotites, and the compositions of mantle source regions for the primitive Apollo 15 green glasses, basaltic shergottites and non-cumulate eucrites calculated assuming a $\Delta^{57}Fe_{Melt\text{-}Mantle}$ of 0.07‰ (see text). The grey field is the range of chondritic meteorites.

in phase transitions and bond stiffening that changes the sign of metal–silicate fraction factors[18,41]. Additional fractionation via the disproportionation of Fe^{2+} by bridgmanite is possible[17], but probably relevant only for Earth. Overall, our results predict δ^{57}Fe for chondrites ≈ Earth > the Moon > Mars ≈ 4 Vesta. Conversely, our results can also explain the isotopically heavy δ^{57}Fe of magmatic Fe meteorites[12,13] (Fig. 1) through the core formation process.

Causes of planetary iron isotope variability

Previous models have postulated that Fe isotope variability among planetary bodies reflects fractionation during the giant impact[4], accretion from the Solar nebula[14], and/or disproportionation of Fe^{2+} in Earth's deep mantle[17], all of which act to concentrate heavy Fe isotopes in mantles. Our results predict that core formation concentrates light Fe in planetary mantles (Fig. 2), although none of these processes is mutually exclusive. Two confounding issues are the uncertainty in estimating the δ^{57}Fe of bulk planetary mantles because no mantle samples currently exist and that planetary mantles may be heterogeneous. Therefore, it is important to estimate the degree to which planetary samples record the core formation process.

In most studies the assumption is made that in extraterrestrial settings, where there is little to no Fe^{3+}, basalts faithfully record the δ^{57}Fe of the mantle from which they melted. In terrestrial systems this is not the case, as mantle partial melting and crystal fractionation result in ^{57}Fe enrichments in the melt[42–45]. A clear example of this is the 0.11 ± 0.04‰ difference between MORBs and abyssal peridotites. However, Dauphas *et al.*[42] showed that only about 1/3 of this difference can be attributed to the effects of Fe^{3+}, leaving a 0.07‰ ± 0.03‰ difference presumably attributable to the differences in average Fe^{2+} bonding environment between MORB magmas and the minerals in their sources, assuming equilibrium partial melting and a constant degree of melting. This Fe^{3+}-free isotope fractionation is supported by the observation of significant δ^{57}Fe variations from −0.03‰ to 0.35‰ in lunar basalts (Fig. 1) where Fe^{3+} does not exist. Importantly, the variations in δ^{57}Fe in lunar magmas correlate with increasing TiO_2 content[4], a hallmark signature of lunar magma ocean crystallization[46–48] (Supplementary Fig. 3). These observations strongly argue for Fe isotope fractionation between minerals and melts in Fe^{3+}-free systems and this must be accounted for when estimating the δ^{57}Fe of planetary mantles.

We used the inferred 0.07‰ δ^{57}Fe difference between Fe^{3+}-free melts and their mantle sources to estimate the δ^{57}Fe of mantle source regions using planetary basalt data. This is a first-order estimate because individual mineral-melt isotopic fractionation factors are not known, nor is the style, degree and temperature of partial melting for most planetary basalts. We calculate that the basaltic shergottites and non-cumulate eucrites are derived from mantle source regions ranging in δ^{57}Fe from −0.14‰ to 0.03‰ and −0.11‰ to 0.02‰, respectively (Fig. 3). We used the δ^{57}Fe of the Apollo 15 green glasses[4] to estimate the δ^{57}Fe of a primitive lunar mantle source region to be −0.15‰ to −0.05‰. The Apollo 15 green glasses are geochemically the most primitive known lunar

magmas[49,50], so they are more likely to record a source region with a δ^{57}Fe similar to the bulk silicate Moon than the more evolved low-Ti mare basalts. In all three cases, these calculated mantle δ^{57}Fe values overlap with the range in mantle values predicted by our experimental results (Fig. 3), providing independent support for our model.

Our model suggests that the near-chondritic δ^{57}Fe of the shergottites, eucrites and the primitive Apollo 15 green volcanic glasses is not a reflection of chondritic mantles, but rather it is consistent with the balancing of light Fe isotope enrichment in the bulk silicate mantles during core formation with subsequent heavy Fe isotope enrichments during both magma ocean crystallization and mantle melting. Fractional crystallization of isotopically light magma oceans will create a heterogeneous mantle that becomes heavier as crystallization proceeds[5], as evidenced by lunar basalt data. Later partial melting will give rise to magmas further enriched in heavy Fe isotopes. Mantle convection has undoubtedly mixed away some of the δ^{57}Fe heterogeneity produced by magma ocean crystallization and mineral-melt fractionation in systems with variable Fe^{2+}/Fe^{3+} needs further investigation before the effects of magmatic processes on Fe isotope fractionation can be fully understood. However, our model for Solar System-wide fractionation during core formation can account for planetary differences in Fe isotopes without the need for the bulk planet (core + mantle) Fe isotope ratio to be different from the chondrite value.

Methods

Methods, including statements of data availability and any associated accession codes and references, are available in the online version of this paper.

Received 15 March 2016; accepted 18 January 2017; published online 20 February 2017

References

1. Young, E. D. *et al*. Oxygen isotopic evidence for vigorous mixing during the Moon-forming giant impact. *Science* **351,** 493–496 (2016).
2. Zhang, J. J., Dauphas, N., Davis, A. M., Leya, I. & Fedkin, A. The proto-Earth as a significant source of lunar material. *Nat. Geosci.* **5,** 251–255 (2012).
3. Lugmair, G. W. & Shukolyukov, A. Early Solar System timescales according to ^{53}Mn-^{53}Cr systematics. *Geochim. Cosmochim. Acta* **62,** 2863–2886 (1998).
4. Poitrasson, F., Halliday, A. N., Lee, D. C., Levasseur, S. & Teutsch, N. Iron isotope differences between Earth, Moon, Mars and Vesta as possible records of contrasted accretion mechanisms. *Earth Planet. Sci. Lett.* **223,** 253–266 (2004).
5. Weyer, S. *et al*. Iron isotope fractionation during planetary differentiation. *Earth Planet. Sci. Lett.* **240,** 251–264 (2005).
6. Schoenberg, R. & von Blanckenburg, F. Modes of planetary-scale Fe isotope fractionation. *Earth Planet. Sci. Lett.* **252,** 342–359 (2006).
7. Teng, F. Z., Dauphas, N., Huang, S. C. & Marty, B. Iron isotopic systematics of oceanic basalts. *Geochim. Cosmochim. Acta* **107,** 12–26 (2013).
8. Craddock, P. R., Warren, J. M. & Dauphas, N. Abyssal peridotites reveal the near-chondritic Fe isotopic composition of the Earth. *Earth Planet. Sci. Lett.* **365,** 63–76 (2013).
9. Wang, K. *et al*. Iron isotope fractionation in planetary crusts. *Geochim. Cosmochim. Acta* **89,** 31–45 (2012).
10. Liu, Y. *et al*. Oxygen and iron isotope constraints on near-surface fractionation effects and the composition of lunar mare basalt source regions. *Geochim. Cosmochim. Acta* **74,** 6249–6262 (2010).
11. Craddock, P. R. & Dauphas, N. Iron isotopic compositions of geological reference materials and chondrites. *Geostand. Geoanal. Res.* **35,** 101–123 (2011).
12. Williams, H. M. *et al*. Fe isotope fractionation in iron meteorites: new insights into metal-sulphide segregation and planetary accretion. *Earth Planet. Sci. Lett.* **250,** 486–500 (2006).
13. Poitrasson, F., Levasseur, S. & Teutsch, N. Significance of iron isotope mineral fractionation in pallasites and iron meteorites for the core-mantle differentiation of terrestrial planets. *Earth Planet. Sci. Lett.* **234,** 151–164 (2005).
14. Sossi, P. A., Nebel, O., Anand, M. & Poitrasson, F. On the iron isotope composition of Mars and volatile depletion in the terrestrial planets. *Earth Planet. Sci. Lett.* **449,** 360–371 (2016).
15. Scott, E. R. D. Chemical fractionation in iron meteorites and its interpretation. *Geochim. Cosmochim. Acta* **36,** 1205–1236 (1972).
16. Poitrasson, F. Does planetary differentiation really fractionate iron isotopes? *Earth Planet. Sci. Lett.* **256,** 484–492 (2007).
17. Williams, H. M., Wood, B. J., Wade, J., Frost, D. J. & Tuff, J. Isotopic evidence for internal oxidation of the Earth's mantle during accretion. *Earth Planet. Sci. Lett.* **321,** 54–63 (2012).
18. Polyakov, V. B. Equilibrium iron isotope fractionation at core–mantle boundary conditions. *Science* **323,** 912–914 (2009).
19. Georg, R. B., Halliday, A. N., Schauble, E. A. & Reynolds, B. C. Silicon in the Earth's core. *Nature* **447,** 1102–1106 (2007).
20. Poitrasson, F., Roskosz, M. & Corgne, A. No iron isotope fractionation between molten alloys and silicate melt to 2000 degrees C and 7.7 GPa: experimental evidence and implications for planetary differentiation and accretion. *Earth Planet. Sci. Lett.* **278,** 376–385 (2009).
21. Hin, R. C., Schmidt, M. W. & Bourdon, B. Experimental evidence for the absence of iron isotope fractionation between metal and silicate liquids at 1 GPa and 1250–1300 °C and its cosmochemical consequences. *Geochim. Cosmochim. Acta* **93,** 164–181 (2012).
22. Shahar, A. *et al*. Sulfur-controlled iron isotope fractionation experiments of core formation in planetary bodies. *Geochim. Cosmochim. Acta* **150,** 253–264 (2015).
23. Badro, J., Cote, A. S. & Brodholt, J. P. A seismologically consistent compositional model of Earth's core. *Proc. Natl Acad. Sci. USA* **111,** 7542–7545 (2014).
24. Shahar, A., Elardo, S. M. & Macris, C. A. in *Non-Traditional Stable Isotopes* Vol. 82 (eds Teng, F. Z., Dauphas, N. & Watkins, J. M.) Ch. 3, 65–84 (Reviews in Mineralogy and Geochemistry, Mineralogical Society of America, 2017).
25. Hume-Rothery, W. *The Structures of Alloys of Iron: An Elementary Introduction* (Elsevier, 2013).
26. Li, J. & Agee, C. B. The effect of pressure, temperature, oxygen fugacity and composition on partitioning of nickel and cobalt between liquid Fe-Ni-S alloy and liquid silicate: implications for the Earth's core formation. *Geochim. Cosmochim. Acta* **65,** 1821–1832 (2001).
27. McDonough, W. F. & Sun, S. S. The composition of the Earth. *Chem. Geol.* **120,** 223–253 (1995).
28. Righter, K. & Drake, M. J. Core formation in Earth's Moon, Mars, and Vesta. *Icarus* **124,** 513–529 (1996).
29. Dreibus, G. & Wänke, H. Mars, a volatile-rich planet. *Hans Suess Festschrift* **20,** 367–381 (1985).
30. O'Neill, H. S. C. The origin of the Moon and the early history of the Earth - a chemical model. Part 1: the Moon. *Geochim. Cosmochim. Acta* **55,** 1135–1157 (1991).
31. Hertogen, J., Vizgirda, J. & Anders, E. Composition of the parent body of eucritic meteorites. *Bull. Am. Astronom. Soc.* **9,** 458 (1977).
32. Anderson, D. L. Internal constitution of Mars. *J. Geophys. Res.* **77,** 789–795 (1972).
33. Corgne, A., Siebert, J. & Badro, J. Oxygen as a light element: a solution to single-stage core formation. *Earth Planet. Sci. Lett.* **288,** 108–114 (2009).
34. Siebert, J., Badro, J., Antonangeli, D. & Ryerson, F. J. Terrestrial accretion under oxidizing conditions. *Science* **339,** 1194–1197 (2013).
35. O'Rourke, J. G. & Stevenson, D. J. Powering Earth's dynamo with magnesium precipitation from the core. *Nature* **529,** 387–389 (2016).
36. Steenstra, E. S., Rai, N., Knibbe, J. S., Lin, Y. H. & van Westrenen, W. New geochemical models of core formation in the Moon from metal-silicate partitioning of 15 siderophile elements. *Earth Planet. Sci. Lett.* **441,** 1–9 (2016).
37. Pringle, E. A., Savage, P. S., Badro, J., Barrat, J. A. & Moynier, F. Redox state during core formation on asteroid 4-Vesta. *Earth Planet. Sci. Lett.* **373,** 75–82 (2013).
38. Righter, K. & Chabot, N. L. Moderately and slightly siderophile element constraints on the depth and extent of melting in early Mars. *Meteorit. Planet. Sci.* **46,** 157–176 (2011).
39. Steenstra, E. S., Knibbe, J. S., Rai, N. & van Westrenen, W. Constraints on core formation in Vesta from metal-silicate partitioning of siderophile elements. *Geochim. Cosmochim. Acta* **177,** 48–61 (2016).
40. Russell, C. T. *et al*. Dawn at Vesta: testing the protoplanetary paradigm. *Science* **336,** 684–686 (2012).
41. Shahar, A. *et al*. Pressure-dependent isotopic composition of iron alloys. *Science* **352,** 580–582 (2016).
42. Dauphas, N. *et al*. Magma redox and structural controls on iron isotope variations in Earth's mantle and crust. *Earth Planet. Sci. Lett.* **398,** 127–140 (2014).
43. Teng, F. Z., Dauphas, N. & Helz, R. T. Iron isotope fractionation during magmatic differentiation in Kilauea Iki Lava Lake. *Science* **320,** 1620–1622 (2008).
44. Weyer, S. What drives iron isotope fractionation in magma? *Science* **320,** 1600–1601 (2008).

45. Sossi, P. A., Foden, J. D. & Halverson, G. P. Redox-controlled iron isotope fractionation during magmatic differentiation: an example from the Red Hill intrusion, S. Tasmania. *Contrib. Mineral. Petrol.* **164,** 757–772 (2012).
46. Snyder, G. A., Taylor, L. A. & Neal, C. R. A chemical model for generating the sources of mare basalts: combined equilibrium and fractional crystallization of the lunar magmasphere. *Geochim. Cosmochim. Acta* **56,** 3809–3823 (1992).
47. Hess, P. C. & Parmentier, E. M. A model for the thermal and chemical evolution of the Moon's interior: implications for the onset of mare volcanism. *Earth Planet. Sci. Lett.* **134,** 501–514 (1995).
48. Elardo, S. M., Draper, D. S. & Shearer, C. K. Lunar magma ocean crystallization revisited: bulk composition, early cumulate mineralogy, and the source regions of the highlands Mg-suite. *Geochim. Cosmochim. Acta* **75,** 3024–3045 (2011).
49. Shearer, C. K. & Papike, J. J. Basaltic magmatism on the Moon: a perspective from volcanic picritic glass beads. *Geochim. Cosmochim. Acta* **57,** 4785–4812 (1993).
50. Hess, P. C. On the source regions for mare picrite glasses. *J. Geophys. Res.* **105,** 4347–4360 (2000).

Acknowledgements

We are grateful to T. D. Mock, M. F. Horan, C. K. I. Sio and J. A. Armstrong for assistance with clean laboratory chemistry, mass spectrometry and SDD–EDS analyses. J. Labidi is thanked for providing comments on an early version of the manuscript. This work was funded by NSF grant EAR-1321858 to A.S.

Author contributions

Both authors contributed equally to this work.

Additional information

Supplementary information is available in the online version of the paper. Reprints and permissions information is available online at www.nature.com/reprints. Correspondence and requests for materials should be addressed to S.M.E.

Competing financial interests

The authors declare no competing financial interests.

Methods

Experimental methods. Experimental silicate starting materials were modelled after the 'Earth-like' peridotite starting composition of Shahar and colleagues[22]. Our starting mix was synthesized from reagent-grade SiO_2, Al_2O_3, MgO, $CaSiO_3$ and synthetic fayalite, such that all Fe in the silicate was nominally ferrous[51,52]. A small amount ($\ll$1% of the total Fe in the silicate) was added as $^{54}Fe_2O_3$ such that the three-isotope exchange method could be used to assess isotopic equilibrium (see below). Starting materials were ground and homogenized in a multi-step process under ethanol with an agate mortar and pestle. Metal starting materials were mixtures of Alfa Aesar 99.999% pure Fe and Ni metals. For Ni-free experiments, an aliquot of the peridotite was added to Fe metal and mixed dry. For Ni-bearing experiments, the Fe–Ni mixture was made first and then added to an aliquot of the peridotite and mixed dry. The peridotite–metal ratio for all starting materials was ~68:32 by weight to approximate the mantle–core mass ratio of Earth[27]. All starting materials were stored in a ~110 °C drying oven until use.

Starting materials were loaded into graphite capsules and were stored in a drying oven until use. Piston-cylinder experiments were conducted in an end-loaded Boyd–England piston cylinder at the Geophysical Laboratory (GL), Carnegie Institution of Washington. Half-inch talc-Pyrex cells with graphite heaters were used as a pressure medium and all other inner parts were crushable MgO pre-fired at 1,000 °C, with the exception of the thermocouple sheath, which was hard-fired Al_2O_3. Temperature was monitored with a Type C W-Re thermocouple. Both Pb foil and a Mo-disulfide suspension were used as lubrication in the pressure vessel. Experiments were pressurized cold to the pressure of interest before being heated to 1,450 °C at 100 °C min^{-1} and then to 1,850 °C at 50 °C min^{-1}. Pressure was manually maintained during heating. All experiments were conducted at 1 GPa and 1,850 °C to ensure that both the metal and silicate phases were completely molten. Experimental durations ranged from 0.5 to 3 h and were terminated by cutting power to the heater. On completion of the experiment, samples were split with one fraction being mounted in epoxy and polished flat for silicon drift detector–energy-dispersive spectrometry (SDD–EDS) analyses and the other fraction being reserved for isotopic analyses.

Silicon drift detector–energy-dispersive spectrometry (SDD–EDS) analyses. Chemical analyses of silicate and metal phases in our experimental run products were conducted using the JEOL 6500F field-emission scanning electron microscope at GL equipped with an Oxford X-Max 80 mm^2 Si drift detector. Unlike traditional EDS analysis, which is semiquantitative at best, Si drift detectors allow for fully quantitative and standardized chemical analyses for major and most minor elements with similar accuracy and precision to wavelength dispersive spectroscopy analysis[53,54]. Experimental samples and a piece of Alfa Aesar 99.995% pure Fe metal rod were mounted in epoxy and polished flat. Immediately prior to SDD–EDS analysis, samples were cleaned with an Evactron 25/45 oxygen RF plasma cleaner to remove surface carbon contamination before being coated with a thin (~1 nm) layer of iridium. Despite this cleaning process, some carbon contamination survived through to the analyses.

Metal analyses were conducted by collecting an EDS spectrum for 50 s at an operating voltage of 15 kV and a beam current of ~1 nA with a ~12 × 12 μm raster size. Analyses of the Alfa Aesar 99.995% pure Fe metal rod provided a baseline for the amount of surface carbon contamination present. The carbon content of experimental Fe alloys was calculated by subtracting the calculated amount of carbon contamination from the total carbon measured. The amount of carbon contamination is determined by analysis of the Fe metal rod and comparison of the intensity correction factor (that is, a matrix correction) applied to the apparent concentration calculated from the k-ratio. If the intensity correction factors calculated for the Alfa Aesar 99.995% pure Fe metal rod and the experimental alloys were identical, as was often the case, the amount of carbon in wt% measured for the Fe metal rod can simply be subtracted from the carbon measured for experimental alloys. This correction typically resulted in analytical totals near 100% for Fe alloys (Supplementary Table 1).

Silicate analyses were made using the SDD–EDS detector in quantitative mapping mode, which was necessary due to the coarse-grained quench crystals typical of experiments on peridotite and other ultramafic silicate compositions. Analyses were made over 115 × 86 μm areas at 15 kV, a beam current of ~1 nA, and a 1 ms per pixel counting time. Standards for all SDD–EDS analyses were pyrope for Si, diopside for Ca, cossyrite for Fe, an aluminous enstatite for Mg and Al, Ni-bearing olivine for Ni, and graphite for C. The quality of the standardization and the success of the C correction procedure were checked against a number of secondary standards including a basaltic glass, Fe metal, Ni metal, Si metal, SiC, Ti metal, TiC, V metal, VC and Si-bearing Fe_3C.

Multiple collector inductively coupled plasma mass spectrometer (MC-ICP-MS) analyses. The remaining half of each experimental run product was crushed in an agate mortar and pestle. The Fe alloy and silicate phases were hand-picked under a binocular microscope and separated easily. The silicate fractions were checked for purity with a strong magnet to ensure no contamination from small Fe alloy inclusions. Phase dissolutions and anion exchange chromatography followed the 'short column' procedures of Craddock and Dauphas[11]. Dissolutions involved a three-step process: 1 ml of concentrated HF + 0.5 ml of concentrated HNO_3; 0.75 ml of concentrated HCl + 0.25 ml of concentrated HNO_3; and 1 ml concentrated HCl + 0.5 ml concentrated HNO_3. Dissolutions were conducted in closed Savillex beakers on a hot plate at ~150 °C, and were then dried down before the addition of new acids. After the third step, the samples were dissolved in 0.5–5 ml of 6 M HCl, depending on Fe concentration, for column chemistry. Iron was purified by anion exchange chromatography using 1 ml of BioRad AG-1x8 200–400 mesh pre-cleaned resin and BioRad Poly-Prep short chromatography columns. Between 0.1 and 0.5 ml of sample in 6 M HCl was added to the columns and after elution of matrix elements, the sample was collected in 0. 5M HCl. Purified Fe was then dried down, redissolved in 6 M HCl, and the column chemistry was repeated with new resin and columns to ensure the purity of the sample. Afterward, purified Fe was dissolved in 0.5 ml of 0.4 M HNO_3 for MC-ICP-MS analyses.

Isotopic analyses were conducted in high-resolution mode on the Nu Instruments Plasma II MC-ICP-MS at the Geophysical Laboratory, which has a fixed array of 16 Faraday collectors each with 10^{11} Ω amplifier resistors. Samples and standards were analysed at a concentration of ~4 ppm Fe in 0.4 M HNO_3 solutions. Instrumental mass fractionation was corrected for using sample-standard bracketing with peak height matching to ≤5%. Interferences on $^{54}Fe^+$, $^{56}Fe^+$ and $^{57}Fe^+$ were resolved from ArN^+, ArO^+ and $ArOH^+$, respectively, by operating in high-resolution mode. The bracketing standard used was IRMM-524a, which has an identical isotopic composition to the international Fe standard IRMM-014 (ref. 11). Although experimental starting materials were nominally Cr-free, the $^{53}Cr/^{54}Fe$ ratio of experiment samples was measured to correct for any potential interference on ^{54}Fe by ^{54}Cr (ref. 55). Only one sample (PC 1364 silicate fraction) required a small correction for Cr. Samples were analysed 7–22 times with each analysis consisting of 20 cycles of 4 s integrations. Metal and silicate samples were always measured back to back on the same day. Errors on individual analyses are reported as 2 × s.e.m. (ref. 55).

Assessment of chemical and isotopic equilibrium. The approach to chemical equilibrium in experimental run products was assessed with SDD–EDS analyses. Both metal and silicate phases showed limited chemical variability outside of that produced by analyses of coarse quench textures. Furthermore, the chemical compositions of phases remained relatively constant through a series of identical experiments from 0.5 to 3 h. These results indicate that metal and silicate phases closely approached chemical equilibrium in our experiments.

The approach to isotopic equilibrium in our experiments was assessed with both a time series (Supplementary Fig. 1) and the three-isotope exchange technique[24,56]. As mentioned above, the peridotite starting mix was spiked with a small amount of $^{54}Fe_2O_3$ so as to move the bulk Fe isotopic composition of the system off the terrestrial fractionation line (TFL) and place the initial isotopic compositions of the peridotite and metal dramatically out of equilibrium. During the experiment, the metal and silicate phases re-equilibrate, and when isotopic equilibrium is reached they will both lie on a new mass-dependent secondary fractionation line (SFL). The difference between the TFL and the SFL (with identical slopes) in three-isotope space is expressed as $\Delta^{56}Fe$. When isotopic equilibrium has been reached, the metal and silicate fractions in an experiment should have identical $\Delta^{56}Fe$ values. In Supplementary Fig. 2, we show the $\Delta^{56}Fe$ values of metal and silicate fractions in each experiment. The $\Delta^{56}Fe$ values of the fractions in each experiment are the same within error, indicating our experiments reached isotopic equilibrium. The slight differences in absolute $\Delta^{56}Fe$ between each experiment are a reflection of slightly variable amounts of the ^{54}Fe spike in each experiment and/or difference in the proportions of the isotopically different peridotite and Fe metal reagent, but given the large difference in isotopic compositions of the starting materials (Supplementary Table 2), they are very similar. We conducted a time series of experiments at 0.5, 1, 2 and 3 h in graphite capsules. All experiments were in equilibrium and resulted in similar $\Delta^{57}Fe_{Core-Mantle}$ values, indicating isotopic equilibrium is reached quickly at these pressure and temperature conditions.

Data availability. The authors declare that the data supporting the findings of this study are available within the article and its Supplementary Information files.

References

51. Vander Kaaden, K. E., Agee, C. B. & McCubbin, F. M. Density and compressibility of the molten lunar picritic glasses: implications for the roles of Ti and Fe in the structures of silicate melts. *Geochim. Cosmochim. Acta* **149,** 1–20 (2015).
52. Elardo, S. M., Shearer, C. K., Kaaden, K. E. V., McCubbin, F. M. & Bell, A. S. Petrogenesis of primitive and evolved basalts in a cooling Moon: experimental constraints from the youngest known lunar magmas. *Earth Planet. Sci. Lett.* **422,** 126–137 (2015).

53. Ritchie, N. W. M., Newbury, D. E. & Davis, J. M. EDS measurements of X-ray intensity at WDS precision and accuracy using a silicon drift detector. *Microsc. Microanal.* **18,** 892–904 (2012).
54. Armstrong, J. T. Comparative performance of SDD-EDS and WDS detectors for quantitative analysis of mineral specimens: the next generation of electron microprobe. *Microsc. Microanal.* **20,** 692–693 (2014).
55. Dauphas, N., Pourmand, A. & Teng, F. Z. Routine isotopic analysis of iron by HR-MC-ICPMS: how precise and how accurate? *Chem. Geol.* **267,** 175–184 (2009).
56. Shahar, A., Young, E. D. & Manning, C. E. Equilibrium high-temperature Fe isotope fractionation between fayalite and magnetite: an experimental calibration. *Earth Planet. Sci. Lett.* **268,** 330–338 (2008).